Nano Research

Open Access

Research Article

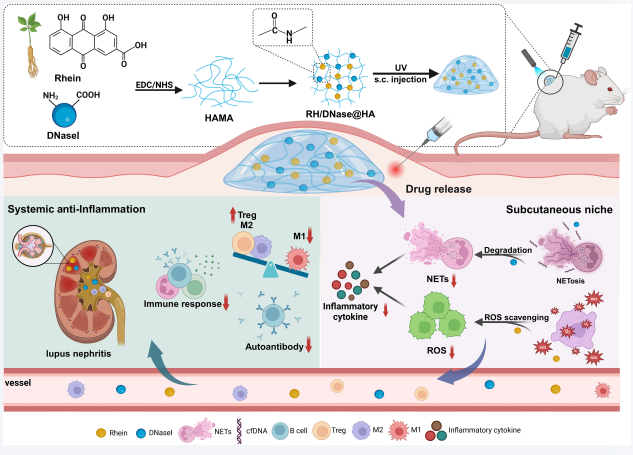
# Subcutaneously injected Chinese herbal hydrogel as a NETs-scavenging niche for restoring immune homeostasis in lupus

Jiawen Wu[1], Shufan Hou[1], Shiwen Ni[2], Mei Yang[2]✉, Chen Dong[2]✉, Yujuan Zhu[2]✉, and Zhifeng Gu[1]✉

[1] *Department of Rheumatology, Affiliated Hospital of Nantong University, Medical School of Nantong University, Nantong 226001, China*
[2] *Research Center of Clinical Medicine, Affiliated Hospital of Nantong University, Medical School of Nantong University, Nantong 226001, China*

**Cite this article:** *Nano Research*, **2026**, *19*, 94908901. https://doi.org/10.26599/NR.2026.94908901

**ABSTRACT:** Systemic lupus erythematosus (SLE) is a chronic inflammatory disease. It is characterized by multisystem involvement and potential damage to multiple organs, especially the kidneys, resulting in a substantial clinical burden. Current treatment strategies, including corticosteroids, biologics, and immunosuppressives, are often limited by their limited efficacy and side effects. Increasing evidence suggests that dysregulated neutrophil extracellular traps (NETs) and systemic inflammatory responses are closely related to the pathogenesis and progression of SLE. This suggests a potential immunomodulatory target. Inspired by the human immune niche, we developed a novel Chinese herbal hydrogel for lupus immunotherapy. By combining Rhein and deoxyribonuclease I (DNase I) with photo-crosslinkable hyaluronic acid, an injectable traditional Chinese medicine hydrogel was obtained. After subcutaneous injection, it can sustainably release active herbal ingredients, regulate systemic inflammation and effectively clear NETs. *In vivo* studies have shown that biomimetic hydrogels can not only improve systemic symptoms but also control renal lesions through sustained systemic intervention therapy. Hydrogel treatment can significantly alleviate the pathological changes related to lupus, reduce the level of inflammatory factors, and expand the number of regulatory T cells. It also improved immune cell infiltration and progression of lupus nephritis, emphasizing its ability to restore systemic immune homeostasis. Notably, transcriptome analysis revealed that hydrogels attenuate SLE by orchestrating down-regulation of neutrophil function and pathogenic processes of inflammation while enhancing antioxidant defense and immunomodulatory signaling. These findings suggest that the traditional Chinese herbal hydrogel system exhibits significant therapeutic potential as a biomimetic immune niche for SLE and may provide a promising platform for lupus treatment.




**KEYWORDS:** systemic lupus erythematosus, neutrophil extracellular traps (NETs) scavenging, Chinese herbal hydrogel, Rhein, immunotherapy

## 1 Introduction

Systemic lupus erythematosus (SLE) is an autoimmune disease, mainly occurring in women of childbearing age [1, 2]. Its pathogenesis is complicated and poses a great challenge for treatment. SLE seriously damages the patient's systemic organs, producing circulating autoantibodies to most organ systems [3]. This is followed by deposition of immune complexes and complement activation in tissues, leading to extensive systemic inflammation [4, 5]. Neutrophils, as important effectors of innate immunity, can produce neutrophil extracellular traps (NETs) after undergoing programmed death [6, 7]. Aberrant production of NETs has an important role in autoimmunity [8]. NETs release autoantigens which could directly or indirectly aggravate the pathophysiology and clinical symptomatology in autoimmune disease. Abnormal accumulation of NETs has been reported to

**Received:** April 12, 2026; **Revised:** May 26, 2026
**Accepted:** May 29, 2026

✉Address correspondence to Mei Yang, yangmei@ntu.edu.cn; Chen Dong, dongchensc@126.com; Yujuan Zhu, yujuanzhu@ntu.edu.cn; Zhifeng Gu, guzf@ntu.edu.cn

cause lupus nephritis, a refractory complication of lupus that causes serious organ damage [9, 10]. Because it is chronically recurring and has hard-to-control complications, SLE not only causes disease burden to patients but also leads to great economic and social burden. In addition, although conventional therapeutic approaches like glucocorticoids are capable of controlling the disease in part, frequent usage causes serious adverse reactions such as a higher infection rate and osteoporosis which affects the patient's adherence to the treatment [11, 12]. In recent years, new therapeutic strategies in lupus have emerged including biologic drugs or synthetic substances (i.e., lipid nanocarriers [13, 14]). The emergence of such treatment methods has made it possible for targeted treatment of the immune system in the treatment of lupus, overcome drug resistance to a certain extent, and produce stable treatment effects. However, these approaches are still unable to completely reverse the recurrence of SLE, and the cost for a long period of time with repeated medications is relatively expensive. Therefore, there is an urgent need to develop a new therapeutic system addressing the refractory characteristics of SLE.

Herein, we develop a bioinspired immune niche for SLE immunotherapy. Immune niche refers to the dynamic microenvironment in certain tissues or organs, containing immune cells, secreted cytokines, extracellular matrix, and others [15–17]. Via inter-cellular interactions and associated signaling pathways, it plays an essential role in several processes associated with the immune response. It is involved in modulation of immune response, maintenance of immune tolerance and in the incidence and development of several diseases [18–20]. Besides, the Chinese herbal medicine hydrogel system combines the active components in herbs with the hydrogel carrier, which have a high potential for inflammation modulation and immune regulation [21–23]. Based on the physical structure stability and good biocompatibility characteristics of hydrogel, this platform can improve the bioavailability and efficacy of the medicine components, extend its half-life *in vivo* to achieve a prolonged pharmacological effect and reduce the side effects caused by systemic distribution. For chronic and recurrent autoimmune disease like SLE, this approach could reduce dosing frequency without loss of anti-inflammatory potency, thus increasing adherence to therapy as well as its success. However, studies of the immunomodulation effect of Chinese herbal-based hydrogels in SLE are still in their infancy.

In this study, we present a new kind of subcutaneously injected Rhein-loaded hydrogel as a NETs-scavenging niche that could be used for the treatment of SLE through modulating immunity. The injectable herbal hydrogel system (Rh/DNase@HA) was prepared by loading Rhein together with DNase I into hyaluronic acid hydrogel using a chemical crosslinking method. This new strategy is a combination of the anti-inflammatory and immunomodulatory activity of Rhein [24, 25], along with the biocompatible and structurally tunable nature of hyaluronic acid that leads to prolonged delivery of drug molecules. The *in vitro* results showed that it had anti-inflammatory effects, reactive oxygen species (ROS) scavenging ability, and NETs degradation capability. After subcutaneous administration, the loaded hydrogel had extended retention time and stable release profile. In an animal model of SLE disease, application of Rhein-loaded hydrogels led to decreased secretion of inflammatory factors as well as recovery from abnormal cellular immunity patterns. The pathological analysis showed improvement in renal damage, one of the most important complications of SLE. In order to clarify its possible mechanism, we performed RNA sequencing and showed the dual regulation mode of action: Rh/DNase@HA downregulates the pathways related to oxidative stress and NETs formation by neutrophils, while also modulating inflammation-related genes to reestablish immunologic balance. In summary, the Rhein-hydrogel system for subcutaneous application developed in this paper represents an effective lupus treatment strategy inspired by biology, which provides a promising platform for the long-term management of SLE.

## 2 Experimental

### 2.1 Materials

Hyaluronic acid (H874944) was obtained from Macklin (China). Methacrylic anhydride (MA, 276685) and N‑hydroxysuccinimide (NHS, 130672) were purchased from Sigma (USA). 1-(3-Dimethylaminopropyl)-3-ethylcarbodiimide (EDC, A638729) was supplied by Aladdin (China). Rhein (HY-N0105) was acquired from MCE (USA). DNase I (CD14) was obtained from Roche (Switzerland), and 2-hydroxy-2-methylpropiophenone (HMPP) was applied for subsequent experiments.

### 2.2 Preparation of Rh/DNase@HA

Firstly, 4 g of Hyaluronic Acid was dissolved in 200 mL of phosphate-buffered saline (PBS) solution (pH = 7.2–7.4), and the resulting solution was prepared as a 2% (w/v) solution. After complete dissolution, 1 M $NaHCO_3$ was used to adjust the pH of the HA solution to 8.5. Then 12 mL of methacrylic anhydride was slowly added, and the reaction was stirred in an ice-water bath for 4 h, and the pH was monitored every half hour and maintained between 7.5 and 8.5. After the reaction was completed, the unreacted MA in the solution was removed by centrifugation at 3500×*g* for 3 min to obtain the HAMA supernatant. 200 mL of $ddH_2O$ was added to dilute and stirred overnight, then it was dialyzed in 12–14 kDa at 40 °C for 7 days. After dialysis, the pH was adjusted to about 7.2 with 1 M $NaHCO_3$, pre-freezed at −20 °C for one night, and freeze dried, which can be stored for a long time. Subsequently, 200 mg HAMA was dissolved in 4 mL PBS solution. After complete dissolution, 115.09 mg NHS and 218.5 μL EDC were added and stirred for 30 min. Then, 400 μg of DNase I (10 mg/mL) and Rhein were added, and the reaction was stirred for 24 h. Later, the pH level was adjusted to 7–7.5, and dialyzed in 1 kD for 4 days. Water was changed every half day to ensure that NHS and EDC molecules with small molecular weight were filtered out. The solution was pre-freezed at −20 °C for one night, and freeze dried. Finally, before the experiment, 200 mg of Rh/DNase@HA hydrogel product was taken and could be dissolved in PBS according to different concentrations (0.5%, 1.5%, 3%, w/v). 1% HMPP (v/v) was added, vortexed, and oscillated evenly, and irradiated under UV light for 15 s to form a Rh/DNase@HA hydrogel system.

### 2.3 *In vitro* drug release studies

Different concentrations of Rh/DNase@HA (2%, 3%, 5%, w/v) were cured and immersed in PBS buffer solution, placed in a 37 °C constant temperature shaker, and a portion of the release medium was absorbed at a predetermined time point, while filling it with an equal volume of fresh PBS to maintain a constant volume. The Rhein release content in the medium was measured at specific

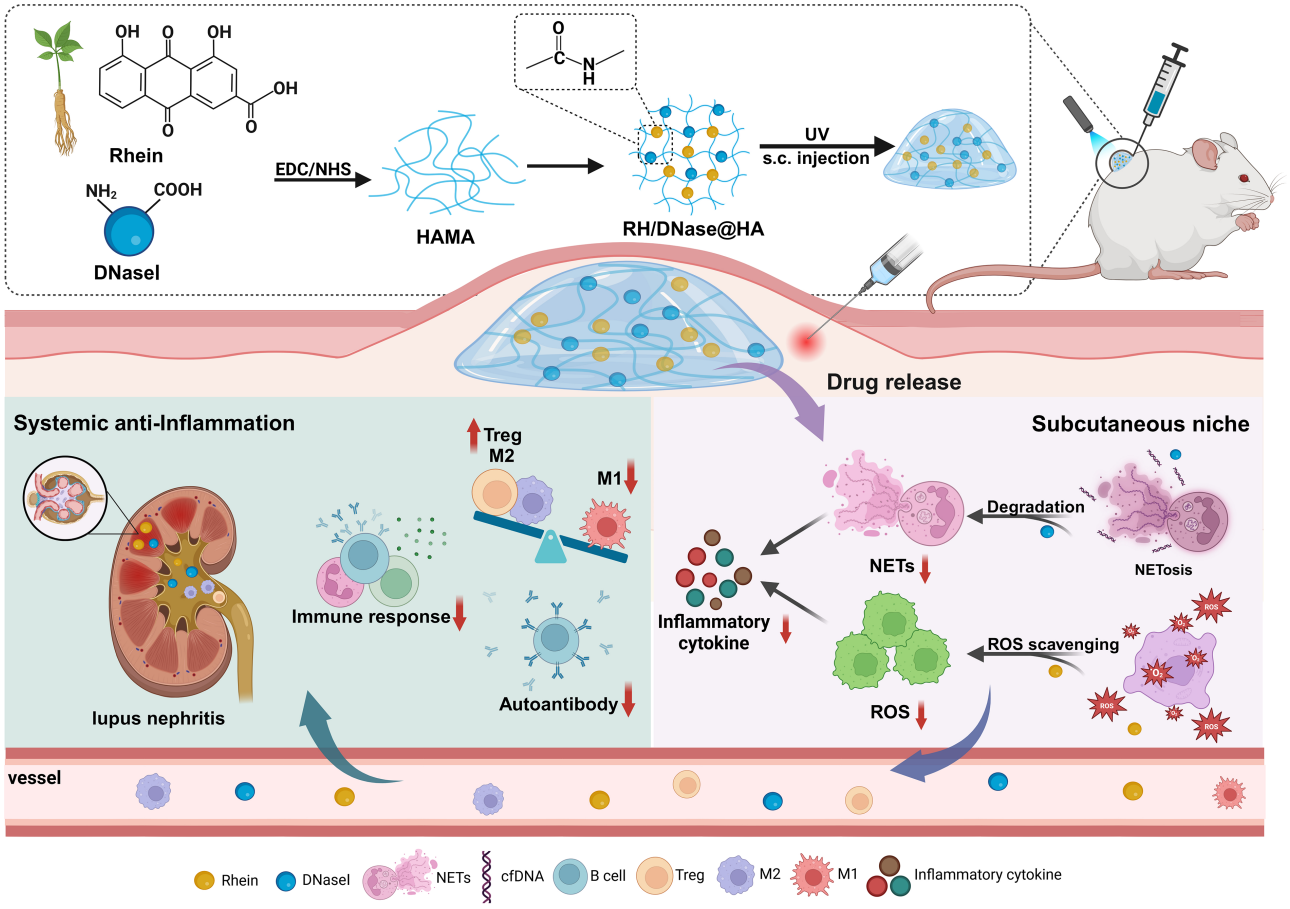



**Figure 1** Schematic representation of the Rh/DNase@HA hydrogel as a NETs-scavenging niche for SLE immunotherapy. Rh/DNase@HA was synthesized by incorporating Rhein and DNase I into a hyaluronic acid methacryloyl (HAMA) network. Upon subcutaneous injection and ultraviolet (UV) cross-linking, the solution forms a stable hydrogel *in situ*, enabling sustained release of therapeutic agents for inflammation modulation and disease alleviation in a murine lupus model (Figure was created with BioRender).

wavelengths using an ultraviolet spectrophotometer.

### 2.4 Biocompatibility of Rh/DNase@HA

*In vitro* experiments: Rh/DNase@HA hydrogels with different concentrations were cured and soaked in high-glucose complete medium for 24 h to obtain drug-conditioned medium. In a 96-well plate, immortalized bone marrow-derived macrophages (iBMDM) cells were cultured for 24 h using different media conditions. According to the cell counting kit-8 (CCK-8) (C6005, NCM Biotech, China) instructions, 10 μL CCK-8 reagent was added to each well, incubated for 1–4 h, and cell activity was detected. In a 6-well plate, human umbilical vein endothelial cells (HUVECs) were cultured for 24 h using different concentrations of conditioned culture medium. Normal high-glucose culture conditions were used as a control. According to the instructions of the Calcein/PI Cell Viability/Cytotoxicity Assay Kit (C2015M, Beyotime, China), staining was performed using Calcein-AM and propidium iodide (PI) dual fluorescence probes, and cell activity was observed under a fluorescence microscope. The dead cells were red and the living cells were green.

*In vivo* experiments: Following the administration of the drug to the mice, the heart, liver, spleen, lung and kidney tissues were preserved, fixed with 4% paraformaldehyde, embedded in paraffin and sectioned. The presence of drug toxicity was then determined by performing hematoxylin and eosin (H&E) staining.

### 2.5 ROS detection

Rh/DNase@HA gels with different concentrations were cured and soaked in high-glucose complete medium for 24 h to obtain drug-conditioned medium. iBMDM cells were cultured in different media conditions at 37 °C with 5% $CO_2$, stimulated with $H_2O_2$ solution (0.2 μL/mL), and a control group was set up. After stimulation, the cells were collected, and the cells were stained away from light using the fluorescent probe 2',7'-dichlorodihydro-fluorescein diacetate (DCFH-DA) according to the instructions of the Reactive Oxygen Species Assay Kit (CA1410, Solarbio, China). Then FACS Calibur (BD Fortessa, USA) and FlowJo software were used to analyze the results.

### 2.6 Photopolymerization hydrogel removes NETs structure

*In vitro* experiments: Human neutrophils were isolated from anticoagulated venous whole blood of adult volunteers. After extracting human peripheral blood neutrophils, the cells were seeded in a 24-well plate at a density of approximately 5 × $10^5$ cells/well, and 14 mm cell crawlers were placed at the same time. Cells were cultured using HAMA, Rh/DNase@HA conditioned medium, or Roswell Park Memorial Institute 1640 (RPMI-1640) medium (PM150110, Pricella, China) containing 10% fetal bovine serum (FBS) (Gibco, USA) and 1% Penicillin-Streptomycin while

NETs were stimulated using phorbol myristate acetate (PMA) (P1585, Sigma, USA) (10 μM). At the same time, there were positive controls (cells stimulated by simple DNase I and PMA) and negative controls (culture medium containing only PMA-stimulated). The cells were incubated at 37 °C with 5% $CO_2$ for 4 h. The supernatant was aspirated, the cell crawlers were washed carefully with PBS, and the sample was stained with myeloperoxidase (MPO) (66177-1-lg, Proteintech, China), citrullinated histone H3 (Cit H3) (ab5103, Abcam, UK), and 4',6-diamidino-2-phenylindole (DAPI) (ab228549, Abcam, UK), followed by washing with PBS. Fluorescence microscope was used for observation.

*In vivo* experiments: Paraffin sections of mouse kidney tissue from different groups were rehydrated, antigen retrieval was performed, and incubated with MPO and Cit H3 antibodies. Fluorescence microscope was used for observation.

### 2.7 Mice and treatments

Female MRL/lpr mice lack *Fas* genes and have symptoms of autoimmune disease, similar to those of SLE patients. MRL/lpr mice showed a significant increase in anti-dsDNA antibodies and suffered from severe nephritis. MRL/mpj were used as their healthy control. In each experiment, female mice were divided into four groups (6 mice per group): Healthy Control, PBS, HAMA, and Rh/DNase@HA (150 μL per mouse), subcutaneously administered at 11 weeks for one month of treatment, once every 10 days.

### 2.8 Flow cytometric analysis of splenic immune cells

A single-cell suspension was prepared from murine spleens and resuspended in fluorescence-activated cell sorting (FACS) buffer. After washing and centrifugation (650*g*, 5 min, room temperature), cells were reconstituted in 100 μL of FACS solution for subsequent staining procedures.

For regulatory T cell (Treg) analysis, cells were first stained with Fixable Viability Dye 455UV (eBioscience, 65-0868-18) and surface markers including CD3-allophycocyanin-cyanine 7 (APC-Cy7) (BD Pharmingen, 557596), CD4-fluorescein isothiocyanate (FITC) (BD Pharmingen, 553729), and CD25-phycoerythrin (PE) (BD Pharmingen, 553866) for 30 min at 4 °C in the dark. Following surface staining, cells were fixed and permeabilized using the FoxP3/Transcription Factor Staining Buffer Set (eBioscience, 00-5523-00), then intracellularly stained with FOXP3-Brilliant Violet 421 (BV421) (BioLegend, 126419). Treg cells were defined as $CD3^+CD4^+CD25^+Foxp3^+$.

For TH1 cell detection, splenocytes were resuspended in complete RPMI-1640 medium and stimulated for 6 h at 37 °C under 5% $CO_2$ with PMA, ionomycin (MCE, HY-13434), and brefeldin A (Sigma, B5936). Cells were then stained with Fixable Viability Dye 455UV and surface antibodies against CD3-APC-Cy7 and CD4-FITC. After fixation, intracellular interferon-gamma (IFN-$\gamma$) was labeled using IFN-$\gamma$-PE (BioLegend, 505807) for 30 min at room temperature in the dark. TH1 cells were gated as $CD3^+CD4^+IFN\gamma^+$.

Macrophage polarization was assessed by staining with Fixable Viability Dye 455UV, F4/80-peridinin-chlorophyll-protein complex-cyanine 5.5 (PerCP-Cy5.5) (eBioscience, 45-4801-80), and CD86-FITC (eBioscience, 11-0862-81) for 30 min at 4 °C. After surface staining, cells were fixed and intracellularly labeled with CD206-PE (BioLegend, 141706) for 30 min at room temperature. M1 macrophage cells were identified as $F4/80^+CD86^+$ and M2 were gated as $F4/80^+CD206^+$.

Neutrophils were labeled with Fixable Viability Dye 455UV, CD45-PerCP-Cy5.5 (BioLegend, 103132), CD11b-PE (BioLegend, 101207), and Ly6G-APC (BioLegend, 127613) by incubation at 4 °C for 30 min. Neutrophils were defined as the $CD45^+CD11b^+Ly6G^+$ cell population.

All samples were acquired on a FACS Fortessa flow cytometer (BD Biosciences) and analyzed using FlowJo software.

### 2.9 Enzyme-linked immunosorbent assay (ELISA)

Mice blood samples were collected using an ethylenediaminetetraacetic acid (EDTA) anticoagulant tube and centrifuged at 3000 rpm for 10 min to extract plasma, and then stored at −80 °C. According to the instructions, plasma levels of anti-dsDNA antibodies, complement component 3 (C3), creatinine and cytokines (including tumor necrosis factor-alpha (TNF-$\alpha$), interleukin-6 (IL-6), interleukin-10 (IL-10), and interleukin-1beta (IL-1$\beta$)) were measured using a Mouse enzyme-linked immunosorbent assay kit (Jingmei Biotechnology, China). In cell anti-inflammatory experiments, the collected cell supernatants were tested for inflammatory factors.

### 2.10 Albuminuria

Mice were placed individually in metabolism cages and urine was collected for 24 h. 24-h urine protein levels in mice were measured using the Bradford Protein Assay Kit (PC0010, Solarbio, China).

### 2.11 Pathology assessment of kidneys

After the treatment, the mice were sacrificed to obtain kidneys. The kidneys were fixed with 4% paraformaldehyde and then embedded in paraffin and sections (4 μm). H&E was used to stain sections to observe glomerular lesions. Immunofluorescent staining was performed with anti-mouse IgG and anti-mouse C3 antibodies using renal paraffin sections.

### 2.12 Statistical analysis

All data are presented as mean ± standard deviation (SD) from no less than three independent experiments, each carried out with triplicate samples. Statistical analysis was performed using one-way analysis of variance (ANOVA) in GraphPad Prism software. A value of $^*P < 0.05$, $^{**}P < 0.01$, $^{***}P < 0.001$ was considered statistically significant.

## 3 Results and discussion

To assess systemic inflammation in SLE patients, we collected blood samples from 27 patients and 11 healthy volunteers. Plasma analysis revealed significantly elevated levels of the inflammatory factors including IL-6, IL-10 and IL-1$\beta$, as well as increased NETs formation in SLE patients compared to controls (Fig. S1 in the Electronic Supplementary Material (ESM)). These findings highlight the critical need to control systemic inflammation and limit NETs accumulation in active lupus patients.

In order to solve this problem, we have developed an injectable hydrogel system designed for locally regulating the immune microenvironment (Fig. 1). HAMA was synthesized by reacting hyaluronic acid with methacrylic anhydride to introduce photo-crosslinkable groups. The lipophilic anthraquinone Rhein is an active component derived from Rhubarb with demonstrated anti-inflammatory and anti-apoptotic properties. It was integrated into the hydrogel along with DNase I, which effectively degrades NETs [26, 27]. Using the EDC/NHS chemistry method, Rhein and DNase

I were covalently bound to modified hyaluronic acid, and then produced a uniform Rh/DNase@HA hydrogel (Fig. 2(a)). Through the photoinitiator and UV light, Rh/DNase@HA hydrogel formed a stable hydrogel through free-radical polymerization, providing a lasting substrate for the construction of artificial immune niche *in vivo*. Successful incorporation of Rhein was visually confirmed by a color intensity gradient corresponding to its concentration (Fig. 2(b)). We further used Fourier transform infrared spectroscopy (FTIR) analysis to verify the covalent conjugation between Rhein and HAMA. Rh/DNase@HA showed C=O and N–H expansion vibration absorption peak enhancement at 2903 and 3425 $cm^{-1}$, indicating the success of synthesis (Fig. 2(c)). Scanning electron microscopy (SEM) confirmed that both active components were entrapped within the hydrogel's porous network (Fig. 2(e)). The mechanical properties of HAMA were tuned by varying its concentration. A 3% HAMA formulation was selected based on a Young's modulus of about 0.11 MPa, because it provided a more physiologically similar mechanical microenvironment in contrast to the overly soft 2% (~ 0.02 MPa) or excessively stiff 5% (~ 0.37 MPa) variants (Fig. 2(d)). Under simulated physiological conditions, Rh/DNase@HA hydrogel could continuously release Rhein over several days (Fig. 2(f)), which also supports its potential for prolonged immunomodulatory effects. In addition, the hydrogel showed excellent biocompatibility, with no significant cytotoxicity observed across a range of concentrations (Figs. 2(g) and 2(h), and Fig. S2 in the ESM). To evaluate the *in vivo* stability of the hydrogel after subcutaneous implantation, we used a cyanine 7 (Cy7)-labeled hydrogel system for fluorescence imaging. Free Cy7 dye was used as the control.

As NETs and ROS are excessively produced in SLE and contribute to inflammatory exacerbation [10, 28, 29], we then evaluated the ability of the Rh/DNase@HA hydrogel system to scavenge NETs and ROS. We first assessed the ROS-scavenging capacity of the hydrogel. $H_2O_2$ stimulation markedly increased intracellular ROS levels in the macrophage cell line RAW264.7, whereas treatment with conditioned medium from Rh/DNase@HA hydrogels significantly attenuated ROS fluorescence intensity. This reduction was quantitatively confirmed from 94.9% to 36.2% by flow cytometry (Figs. 3(a)–3(c)), supporting the hypothesis that the composite hydrogel exerts potent antioxidative activity. To further investigate its anti-inflammatory effects, we examined the polarization of M1 macrophages, which are central mediators of inflammatory responses. Flow cytometry data showed that Rh/DNase@HA significantly reduced the proportion of M1 macrophages from 38.9% to 18.1% (Figs. 3(d) and 3(h)). Consistent with this, ELISA also showed that levels of pro-inflammatory cytokines in cell supernatants were significantly lower in the Rh/DNase@HA group, including TNF-$\alpha$, IL-1$\beta$, and IL-6 (Figs. 3(e)–3(g)). Collectively, these results indicate that Rh/DNase@HA exhibits pronounced anti-inflammatory properties under sustained release conditions. Although short-term UV irradiation has limited impact on protein activity [30], we still

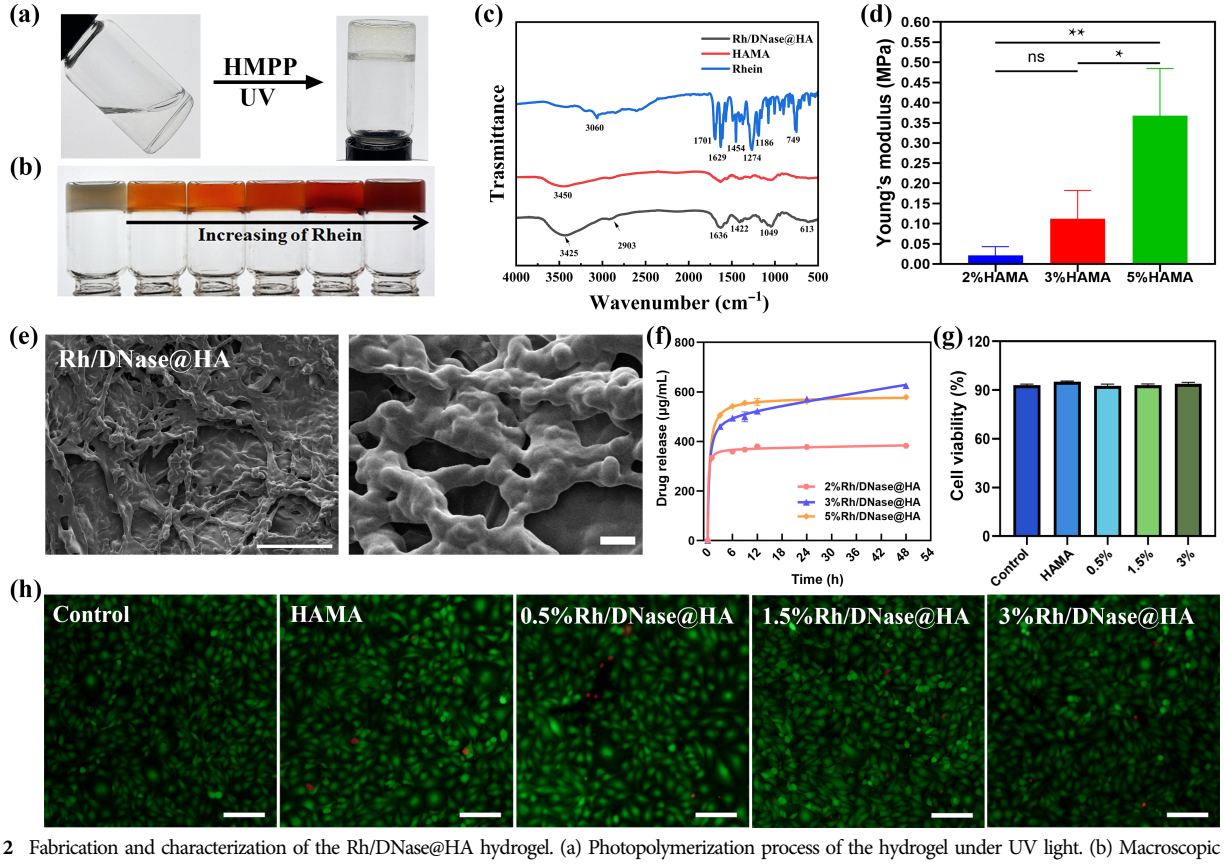



**Figure 2** Fabrication and characterization of the Rh/DNase@HA hydrogel. (a) Photopolymerization process of the hydrogel under UV light. (b) Macroscopic view of hydrogels incorporating increasing concentrations of Rhein (50, 100, 150, 200, 250 μg/mL). (c) FTIR spectra of HAMA, Rhein, and the final Rh/DNase@HA conjugate. (d) Young's modulus of HAMA hydrogels at different polymer concentrations. (e) SEM images of the Rh/DNase@HA hydrogel at different magnifications. Scale bars: 100 μm (left), 10 μm (right). (f) Cumulative *in vitro* release profile of Rhein from Rh/DNase@HA hydrogel ($n$ = 3). (g) Live/dead fluorescence imaging of HUVECs following 24 h incubation with extracts from the Rh/DNase@HA hydrogel. Scale bar: 100 μm. (h) Quantitative analysis of cell viability corresponding to panel (g), assessed by fluorescence intensity. All quantitative data are presented as mean ± SD. *$P$ < 0.05, **$P$ < 0.01.

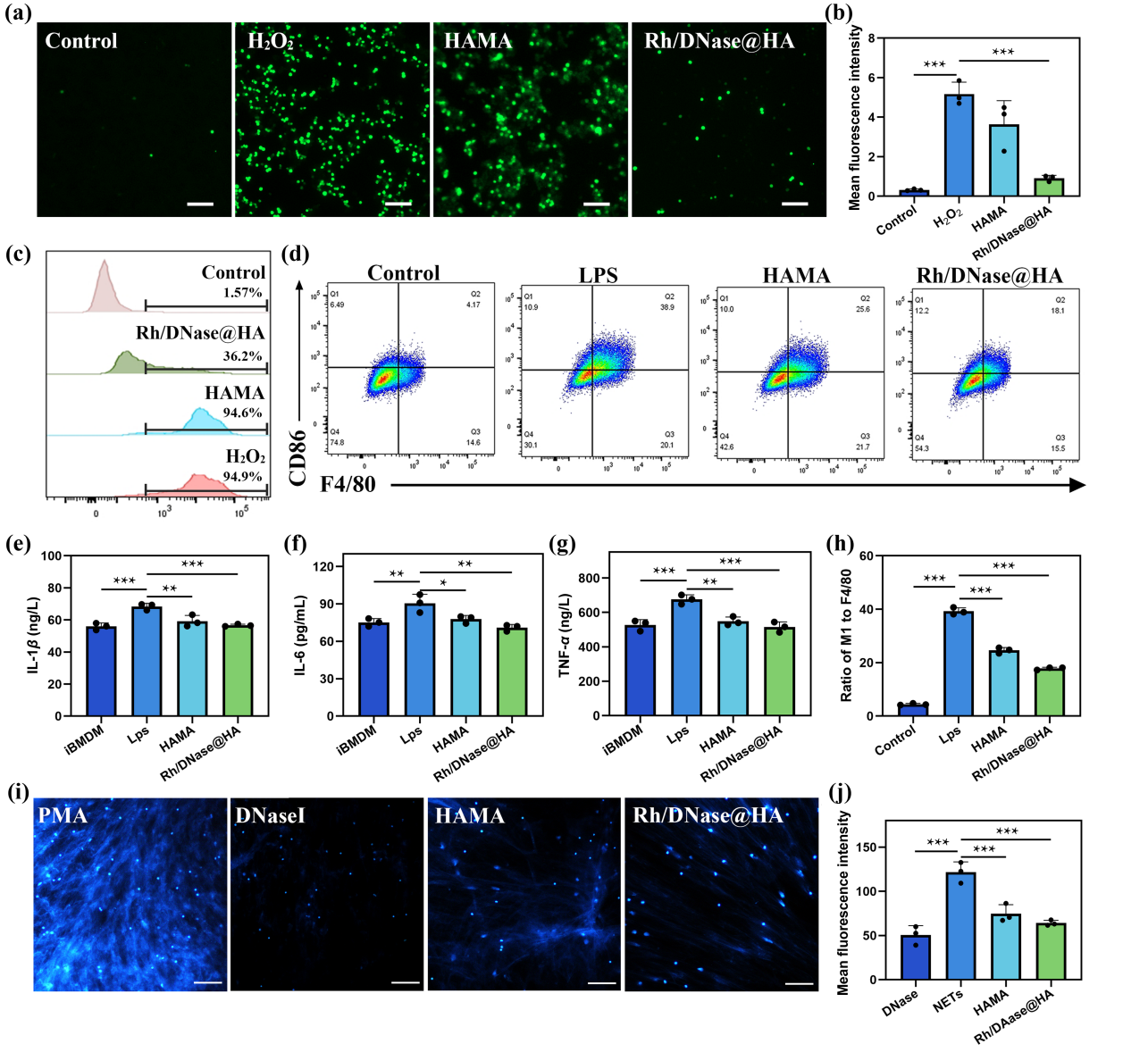



**Figure 3** *In vitro* functional evaluation of Rh/DNase@HA hydrogel. (a) Intracellular ROS detection in macrophages stained with DCFH-DA (green) after treatment with Rh/DNase@HA. (b) Quantitative analysis of ROS fluorescence intensity. (c) Flow cytometric measurement of ROS levels in $H_2O_2$-stimulated iBMDM cells following Rh/DNase@HA treatment. (d) Representative flow cytometry plots showing F4/80$^+$CD86$^+$ M1 macrophage populations. Cytokine concentrations of (e) IL-1$\beta$, (f) IL-6, and (g) TNF-$\alpha$ in cell culture supernatants measured by ELISA. (h) Statistical analysis of M1 macrophage ratio across treatment groups. (i) Fluorescence images of NETs structures stained with DAPI (blue). (j) Quantitative analysis of NETs formation based on fluorescence intensity. Scale bars: 100 μm. Data are presented as mean ± SD ($n$ = 3). *$P$ < 0.05, **$P$ < 0.01, ***$P$ < 0.001.

evaluated the ability of the system to clear NETs *in vitro* to verify whether DNase retains its enzymatic activity after photopolymerization. As shown in Figs. 3(i) and 3(j), and Fig. S3 in the ESM, stimulating neutrophils with PMA for 4 h induced significant NET formation. It appeared as characteristic filamentous structures of decondensed chromatin decorated with granular proteins. Remarkably, after treatment with the Rh/DNase@HA hydrogel, NETs structures resulted in a significant reduction, confirming its anti-NET activity. In short, these findings showed that the Rh/DNase@HA hydrogel can effectively scavenge both ROS and NETs, modulate macrophage polarization, and mitigate inflammatory responses at the cellular level, highlighting its potential as an SLE immunomodulatory therapy.

After confirming the biological efficacy of Rh/DNase@HA *in vitro*, we further investigated its therapeutic potential in SLE murine models using MRL/lpr mice. As shown in Fig. 4(a) and Fig. S4 in the ESM, 10-week-old lupus mice with clinical symptoms were included in the study, and age-matched MRL/mpj mice were used as healthy controls. The hydrogel was administered via subcutaneous injection and then followed by UV-mediated crosslinking on the dorsal neck region, with treatments repeated every 10 days. At 14 weeks of age, blood, kidney, lung, and spleen tissues were taken for comprehensive analysis. By histological pathological staining, we confirmed that transient UV irradiation caused no obvious pathological damage to the local skin of mice (Fig. S5(a) in the ESM). Meanwhile, continuous body weight monitoring during the whole treatment period showed that there was no significant difference between the groups. The histological

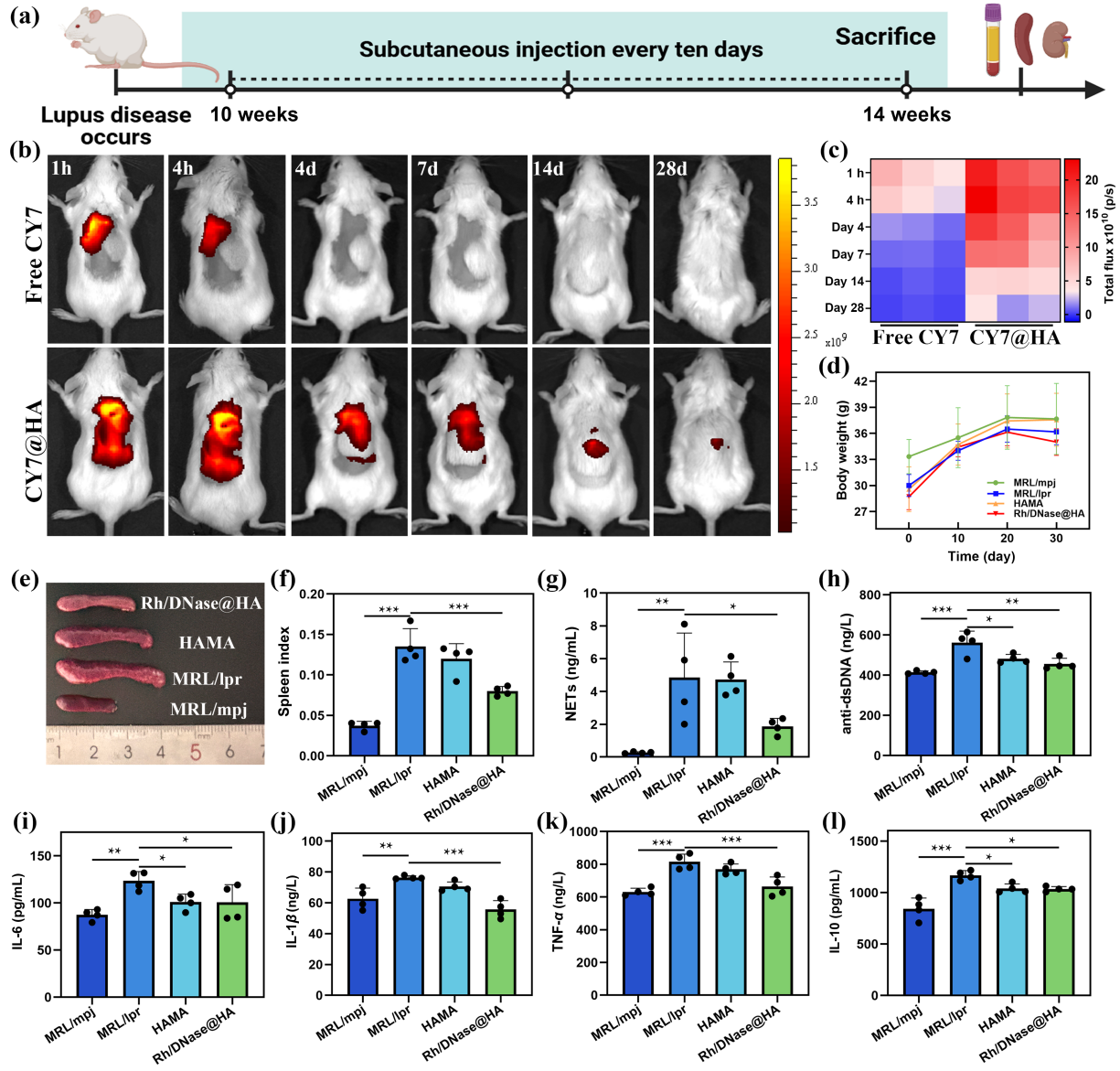



**Figure 4** Therapeutic effects of Rh/DNase@HA in SLE mice. (a) Schematic timeline of the *in vivo* experimental design. Mice were administered PBS, HAMA, or Rh/DNase@HA and sacrificed 4 weeks post-treatment. (b) *In vivo* fluorescence imaging following subcutaneous administration ($n = 3$). (c) Quantification of fluorescence intensity from *in vivo* imaging. (d) Body weight changes in each group throughout the treatment period ($n = 6$). (e) Representative spleen photographs and (f) spleen index across groups. Serum levels of (g) NETs, (h) anti-dsDNA antibodies, and cytokines of (i) IL-6, (j) IL-1$\beta$, (k) TNF-$\alpha$, and (l) IL-10, measured by ELISA. Data are presented as mean ± SD ($n = 4$). $^*P < 0.05$, $^{**}P < 0.01$, $^{***}P < 0.001$.

examination of the main organs confirmed that there was no treatment-related toxicity, emphasizing the good biocompatibility of the hydrogel system (Fig. 4(d) and Fig. S5(b) in the ESM). To evaluate the *in vivo* stability of the hydrogel after subcutaneous implantation, we used a Cy7-labeled hydrogel system for fluorescence imaging. Free Cy7 dye was used as the control. *In vivo* imaging at 1 and 4 h, and days 4, 7, 14, and 28 after injection showed that the retention time of the hydrogel-conjugated fluorophore was significantly prolonged compared with free dye. The signal was always strong for 7 days after injection, and the fluorescent signal could last for even 28 days in the body, compared with the free dye which gradually weakened from the 4th day. This indicates that the hydrogel maintains stability *in situ* and supports its potential for continuous drug release and prolonged efficacy (Figs. 4(b) and 4(c)).

To evaluate the therapeutic impact on lupus manifestations, we first examined the macroscopic morphology of the spleen (Fig. 4(e)). As a central immune organ, splenomegaly is a sign of systemic autoimmunity in mice susceptible to lupus, reflecting the severity of immune activation [31, 32]. The spleen index (spleen weight normalized to body weight) was significantly reduced in Rh/DNase@HA-treated mice compared to PBS or untreated control group, suggesting attenuation of pathological immune responses (Fig. 4(f)). Next, we quantified systemic inflammation and autoimmunity through ELISA determination of serum cytokines and autoantibodies. Rh/DNase@HA treatment led to a significant reduction in NETs content, pro-inflammatory cytokines (TNF-$\alpha$, IL-6, IL-1$\beta$) and immunomodulatory cytokine IL-10, along with a decrease in anti-dsDNA antibody levels, which are serological markers of lupus activity and immune dysregulation

(Figs. 4(g)–4(l)). These findings collectively demonstrate the hydrogel's capacity to mitigate systemic inflammation and autoimmunity in a mouse model of SLE.

In the context of SLE, dysregulated immune activation and breakdown of tolerance mechanisms are often reflected in alterations within splenic immune cell populations. To systematically evaluate these changes, we performed comprehensive flow cytometric analysis of splenic immune cells in lupus-prone mice. Notably, macrophages and TH1 cells, key drivers of inflammatory and cell-mediated immune response, exhibited hyperactivation in lupus-prone mice at disease onset [33–35]. The Rh/DNase@HA hydrogel system significantly reduced abnormally elevated immune cell counts. The proportion of pro-inflammatory macrophage M1 subset was successfully decreased by nearly 3 times, from 9.25% to 3.8%. In contrast, the proportion of M2 macrophages with anti-inflammatory ability increased relatively, reaching 7.56%, which is basically comparable to the healthy control (Figs. 5(a), 5(e), and 5(f), and Fig. S6(a) in the ESM). At the same time, TH1 cells also decreased significantly, from 9.93% to 1.16% (Figs. 5(c) and 5(h), and Fig. S6(c) in the ESM). These results

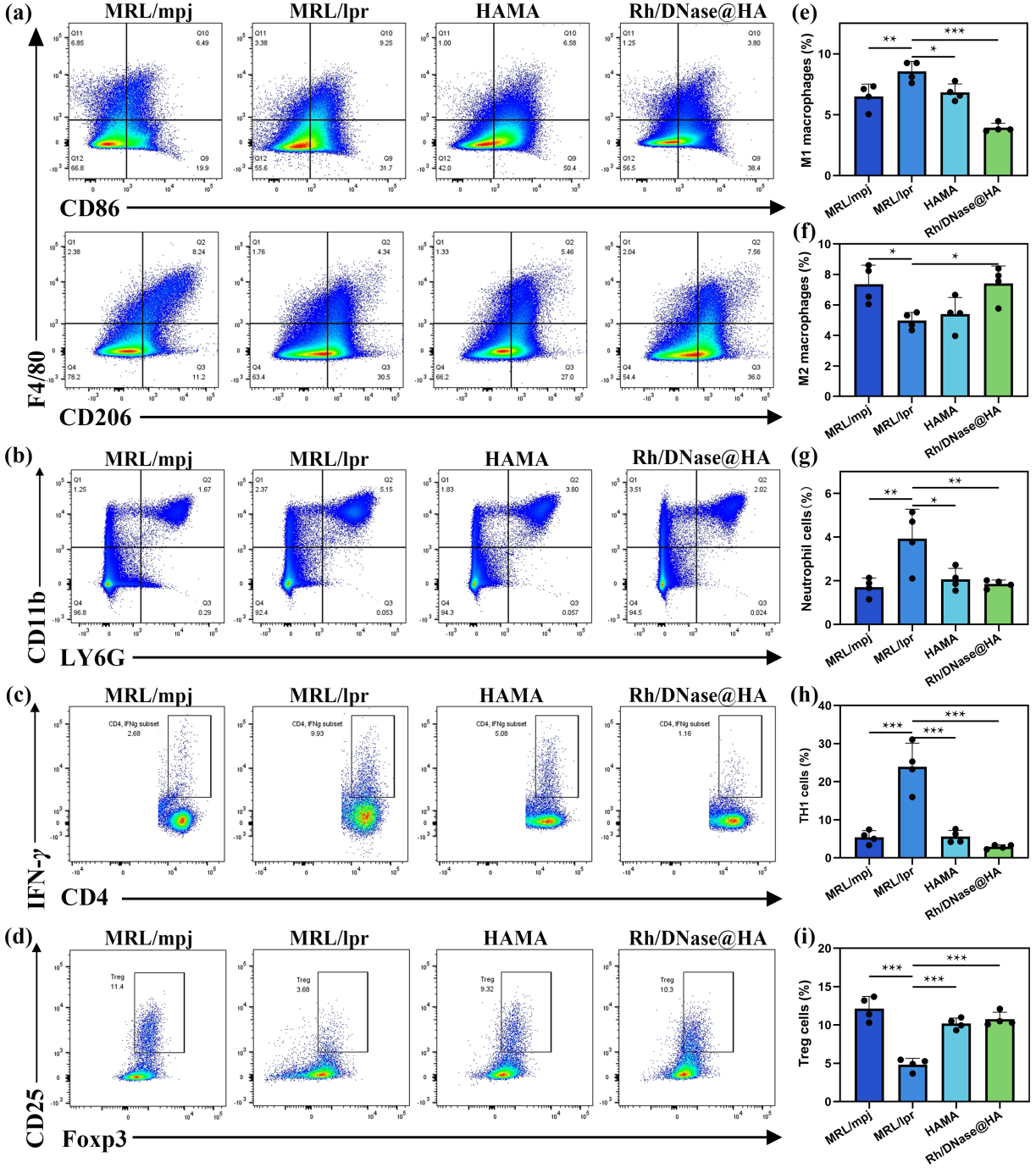



**Figure 5** Modulation of immune cell populations by Rh/DNase@HA in SLE mice. Flow cytometric analysis of (a) macrophage, (b) neutrophil, (c) TH1, and (d) Treg frequencies across experimental groups. Statistical quantification of (e) and (f) macrophage, (g) neutrophil, (h) TH1, and (i) Treg proportions among total immune cells. Data are presented as mean ± SD ($n = 4$). *$P < 0.05$, **$P < 0.01$, ***$P < 0.001$.

jointly prove the efficacy of the Rh/DNase@HA hydrogel system in inhibiting pro-inflammatory reactions. Furthermore, given the established role of neutrophils in influencing autoimmunity through NETs release, we also evaluated their frequency. Treatment with Rh/DNase@HA significantly reduced the proportion of the neutrophil subset, from 5.15% to 2.02%, confirming the effectiveness of targeting this key cell (Figs. 5(b) and 5(g), and Fig. S6(b) in the ESM). In parallel, Treg cells, which maintain immune tolerance and are frequently deficient in lupus [36], showed a significant increase in cell frequency after Rh/DNase@HA treatment. Their proportion rose from 3.68% before treatment to 10.3%, more than tripling, indicating the recovery of immune tolerance pathways (Figs. 5(d) and 5(i), and Fig. S6(d) in the ESM). Compared with MRL/lpr mice, the application of Rh/DNase@HA produced a significant immunomodulation effect. The quantitative analysis of the frequency of immune cell groups further confirms the therapeutic effect of the hydrogel system.

The kidney is the main target organ involved in active SLE. MRL/lpr mice are characterized by severe glomerulonephritis. Its typical pathological manifestations are membrane deposition of complement C3 and IgG, renal vascular lesions and podocyte injury, which together lead to proteinuria and decreased renal function [1, 37]. To assess the renal function after treatment, we collected 24 h urine samples after treatment and measured proteinuria, which is a sensitive indicator of lupus glomerular damage. Compared with the healthy control, untreated lupus mice showed significant proteinuria, and Rh/DNase@HA treatment significantly reduced the level of urine protein (Fig. 6(a)). The serological indicators of kidney function also further verify the therapeutic effect of the hydrogel. The level of complement C3 was negatively correlated with kidney inflammation and increased significantly in treated mice. Compared with the control group, serum creatinine and blood urea nitrogen (BUN), the key indicators of glomerular filtration function, were significantly reduced in the Rh/DNase@HA group, reflecting the improvement of kidney clearance (Figs. 6(b)–6(d)). We further confirmed the protective effect of Rh/DNase@HA on renal lesions in MRL/lpr mice through histopathology and immunofluorescence staining. Histopathological analysis, including H&E staining, Masson's trichrome staining, and periodic acid-Schiff (PAS) staining, showed a comprehensive improvement in renal structure (Figs. 6(g)–6(i)). Treated mice exhibited better kidney morphology, with reduced glomerular mesangial dilation and decreased extracellular matrix protein deposition. Immunofluorescence confirmed the reduction of C3 and IgG deposition on the membrane, and emphasized that the hydrogel reduced tissue damage mediated by immune complexes (Figs. 6(e), 6(f), 6(j), and 6(k)). Meanwhile, staining for NETs-related protein markers in renal tissue further confirmed that the hydrogel can also ameliorate abnormal NETs formation in kidney tissue and effectively alleviate tissue injury (Fig. S7 in the

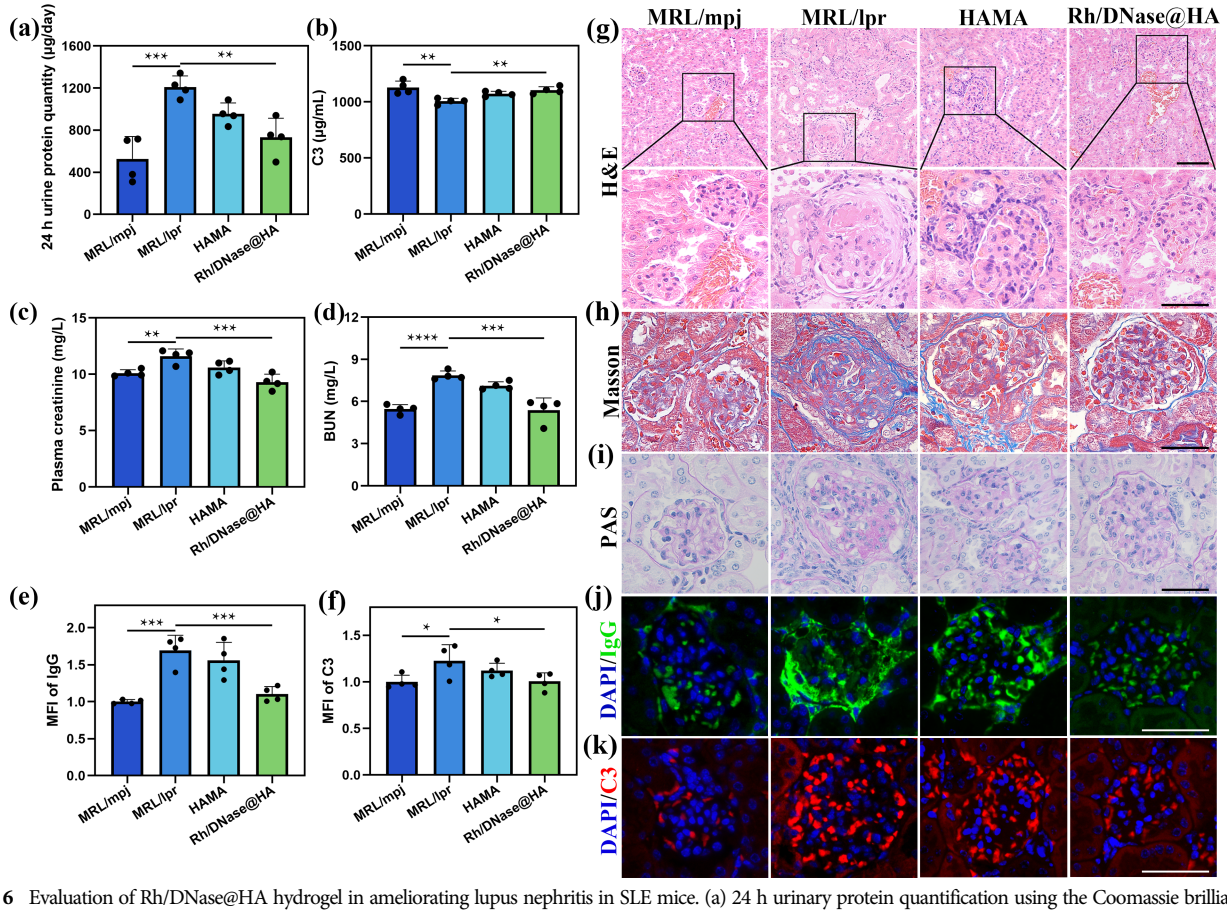



**Figure 6** Evaluation of Rh/DNase@HA hydrogel in ameliorating lupus nephritis in SLE mice. (a) 24 h urinary protein quantification using the Coomassie brilliant blue method ($n$ = 4). Plasma levels of (b) complement C3, (c) creatinine, and (d) BUN measured by ELISA ($n$ = 4). Mean fluorescence intensity of (e) IgG and (f) C3. Representative histological images of kidney sections stained with (g) H&E, (h) Masson's trichrome, and (i) PAS. Scale bars: 100 μm, 50 μm (enlarged version). Representative immunofluorescence images depicting glomerular deposition of (j) IgG and (k) C3. Scale bars: 50 μm. Data are presented as mean ± SD. *$P$ < 0.05, **$P$ < 0.01, ***$P$ < 0.001.

ESM). In conclusion, these findings suggest that the Rh/DNase@HA system can effectively improve the various renal manifestations in SLE, making it a promising candidate for the treatment of autoimmune nephritis and related clinical disorders.

To elucidate the immunotherapeutic mechanisms of the Chinese herbal hydrogel system in SLE, we performed RNA sequencing (RNA-seq) on splenic tissues. Transcriptomic analysis identified 957 downregulated and 110 upregulated genes in the Rh/DNase@HA-treated group compared with the MRL/lpr group ($^*P < 0.05$, $|\log_2(\text{Fold change})| > 1.5$) (Fig. 7(a)). Gene Ontology (GO) enrichment analysis revealed that these differentially expressed genes (DEGs) are closely associated with immune and inflammatory processes, including neutrophil migration and chemotaxis, ROS metabolism, and immune response (Fig. 7(b) and Fig. S8(a) in the ESM). Concurrently, Kyoto Encyclopedia of Genes and Genomes (KEGG) pathway analysis showed significant enrichment in cytokine signaling, complement and coagulation cascade reactions, and phosphoinositide 3-kinase (PI3K)-protein kinase B (Akt) signaling pathway (Fig. 7(c) and Fig. S8(b) in the ESM). Further analysis revealed that Rh/DNase@HA treatment modulates neutrophil activity and attenuates systemic inflammation in SLE mice. Specifically, Rh/DNase@HA upregulated key antioxidant genes (e.g., *Sod3*, *Gpx8*), while downregulating neutrophil-associated genes (e.g., *Mmp9*, *Ly6g*) (Fig. 7(d)), indicating a coordinated mitigation of oxidative stress and neutrophil-driven pathology. Heatmap analysis indicated that genes related to inflammatory responses and immune regulation were also affected. For example, *Tgfb2* and *Tgfb3* were upregulated in the treatment group (Fig. 7(e)). As members of the transforming growth factor-beta (TGF-$\beta$) family, they play a crucial inhibitory role in immune regulation and inflammatory responses. Differences in their expression can affect the differentiation and function of

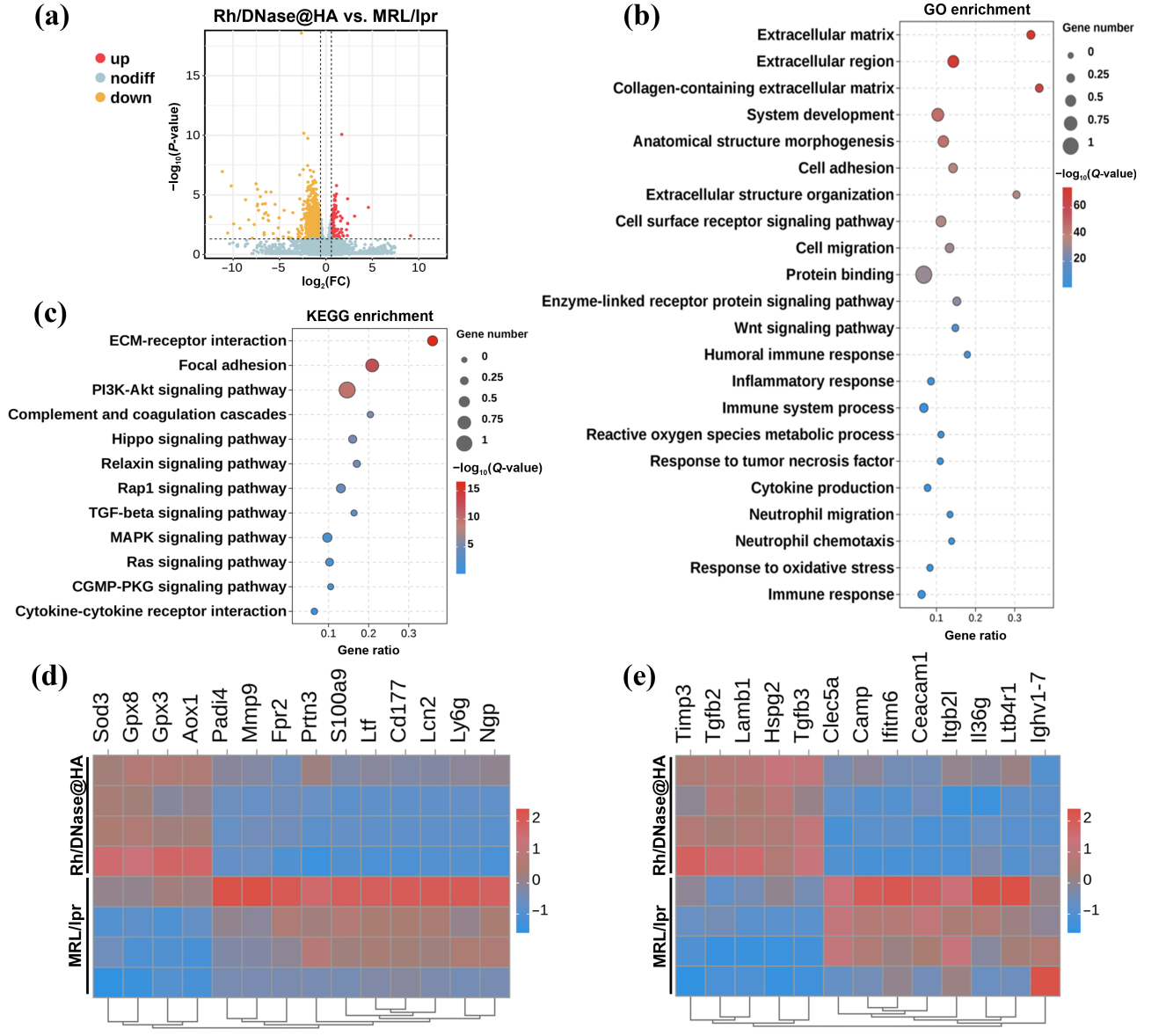



**Figure 7** Therapeutic mechanisms of Rh/DNase@HA hydrogel in SLE mice. (a) Volcano plot analysis of DEGs comparing Rh/DNase@HA-treated and SLE groups. (b) GO and (c) KEGG enrichment of DEGs in the Rh/DNase@HA-treated and SLE groups. (d) Heatmap of neutrophil-related and oxidative stress-related gene expression in the Rh/DNase@HA-treated and SLE groups. (e) Heatmap of inflammation-related and immune-related gene expression in the Rh/DNase@HA-treated and SLE groups.

immune cells, thereby participating in the regulation of inflammatory and immune disorders. These transcriptomic findings indicate that the Rh/DNase@HA hydrogel ameliorates SLE progression by scavenging ROS, attenuating inflammatory signaling, and modulating pivotal pathways implicated in SLE pathogenesis, underscoring its promise as an immunomodulatory therapeutic strategy.

## 4 Conclusions

Here, we constructed a bioinspired multifunctional Chinese herbal hydrogel system serving as a NETs-scavenging niche to achieve SLE immunotherapy. The photo-crosslinkable HAMA matrix is derived from hyaluronic acid, which is widely used in clinical practice, and is used to encapsulate Rhein and DNase I. Rhein is known to have anti-inflammatory properties. Although it may carry a risk of nephrotoxicity, the concentration adopted in this study is consistently within the safe range [38]. In addition, compared with oral administration, local administration minimizes systemic exposure; as a Food and Drug Administration (FDA)-approved drug for the treatment of cystic fibrosis, DNase I has been validated to have long-term safety in human applications [39], which further supports the excellent biocompatibility and biosafety of the entire system. Thus, we have established a biocompatible and immunologically inert drug delivery platform that can release drugs for a long time. The hydrogel mimics the structure of the inflammatory microenvironment with accumulated NETs and exerts a crucial regulatory effect under the combined action of Rhein and DNase I. DNase I functions to target and eliminate existing NETs, thereby directly removing the main source of autoantigens and inflammatory stimuli [26]. In contrast, Rhein acts upstream via ROS scavenging and inflammation inhibition to suppress the formation of new NETs and the driving factors of inflammation [40, 41]. Accordingly, we constructed a dual mechanism of clearance and prevention, allowing Rh/DNase@HA to markedly suppress proinflammatory cytokine secretion, mitigate M1 macrophage polarization, and efficiently degrade NETs structures. In a mouse lupus model, the hydrogel relieved systemic inflammation, ameliorated renal injury, and standardized abnormalities of immune cells, demonstrating its ability to restore the immune system equilibrium in the whole body. The transcriptomic data also showed that the hydrogel influences neutrophil-related genes, oxidative stress, and immune modulating signal transduction, supporting a multi-level mechanism of action.

Despite these promising results, there still exist some shortcomings in this system that need to be taken into consideration. Firstly, even though these immune niche-mimicking functions are conceptually novel, the cellular and molecular crosstalk taking place at the hydrogel-host interface needs more accurate analysis; secondly, the long-term safety and possible immune response for repeated hydrogel administrations should still be assessed on longer terms. Nevertheless, all this said, we believe that the development of Rh/DNase@HA is an interesting combination of bio-inspired materials and traditional Chinese medicine for immune modulation. In fact, it combines scaffolding, continuous release, and multi-target immunoregulation, which provides a new strategy not only for SLE but also possibly for other NETs-associated autoimmune diseases. Optimization of the modular drug loading, enhancement of tissue-specific targeting, and verification of its applicability for human-related disease models are all areas where future work is planned. Further development of this bionic niche could become an adaptable, translatable tool to restore immune homeostasis in autoimmune disease.

**Electronic Supplementary Material**: Supplementary material (more details on patient serology, cell viability, mouse urine protein and organ H&E staining) is available in the online version of this article at https://doi.org/10.26599/NR.2026.94908901.

## Data availability

All data needed to support the conclusions in the paper are presented in the manuscript and/or the Electronic Supplementary Material. Additional data related to this paper may be requested from the corresponding author upon request.

## Acknowledgements

This work was supported by the National Natural Science Foundation of China (Nos. 92574113, 82502178, 82102233, and 82402102), Natural Science Foundation of Jiangsu Province (Nos. BK20241838 and BK20251836), Jiangsu Shuangchuang Talent Program (No. JSSCRC2024596), Jiangsu Provincial Medical Key Discipline Cultivation Unit (No. JSDW202205), Natural Science Foundation of Nantong Municipality (Nos. JC2024029 and JC2023037), Science and Technology Project of Nantong City (No. XNBH00031655), China Postdoctoral Science Foundation (No. 2024M751535), and Jiangsu Funding Program for Excellent Postdoctoral Talent, Jiangsu Provincial Research Hospital (No. YJXYY202204).

## Declaration of competing interest

All the contributing authors report no conflict of interests in this work.

## Author contribution statement

Z. F. G., Y. J. Z., and C. D. conceived the study. J. W. W. performed the experiments and wrote the manuscript. S. F. H., S. W. N., and M. Y. helped to revise the manuscript. All authors read and approved the final manuscript.

## Informed consent

The present research was authorized by the Ethics Committee of the Affiliated Hospital of Nantong University (No. 2025‐K269‐01). Written informed consent was provided from every participant.

## Ethics statement

The animal experiments were carried out following the guidelines of the Nantong University Institutional Committee for the Care and Use of Laboratory Animals and were approved by the Committee on Ethical Use of Animals of Nantong University (Ethical code: S20260120-002).

## Use of AI statement

None.

## References


[1] Siegel, C. H.; Sammaritano, L. R. Systemic lupus erythematosus: A review. *JAMA* **2024**, *331*, 1480–1491.

[2] Lamas, A.; Faria, R.; Marinho, A.; Vasconcelos, C. The mosaic of systemic lupus erythematosus: From autoimmunity to autoinflammation and immunodeficiency and back. *Autoimmun. Rev.* **2024**, *23*, 103675.

[3] Crow, M. K. Pathogenesis of systemic lupus erythematosus: Risks, mechanisms and therapeutic targets. *Ann. Rheum. Dis.* **2023**, *82*, 999–1014.

[4] Patiño-Martinez, E.; Kaplan, M. J. Immunometabolism in systemic lupus erythematosus. *Nat. Rev. Rheumatol.* **2025**, *21*, 377–395.

[5] Arnaud, L.; Chasset, F.; Martin, T. Immunopathogenesis of systemic lupus erythematosus: An update. *Autoimmun. Rev.* **2024**, *23*, 103648.

[6] Herro, R.; Grimes, H. L. The diverse roles of neutrophils from protection to pathogenesis. *Nat. Immunol.* **2024**, *25*, 2209–2219.

[7] Zhang, F. Y.; Xia, Y. D.; Su, J. Y.; Quan, F. S.; Zhou, H. Z.; Li, Q. R.; Feng, Q.; Lin, C.; Wang, D. X.; Jiang, Z. P. Neutrophil diversity and function in health and disease. *Sig. Transduct. Target. Ther.* **2024**, *9*, 343.

[8] Wang, H.; Kim, S. J.; Lei, Y.; Wang, S. H.; Wang, H.; Huang, H.; Zhang, H. J.; Tsung, A. Neutrophil extracellular traps in homeostasis and disease. *Sig. Transduct. Target. Ther.* **2024**, *9*, 235.

[9] Nakazawa, D.; Masuda, S.; Nishibata, Y.; Watanabe-Kusunoki, K.; Tomaru, U.; Ishizu, A. Neutrophils and NETs in kidney disease. *Nat. Rev. Nephrol.* **2025**, *21*, 383–398.

[10] Shu, J. X.; Liang, J. B.; Zeng, L. D.; Zhong, S. P.; Fang, X. L.; Xu, Y. T.; Wu, Y. J.; Huang, X. TREM2 drives neutrophil extracellular traps-induced dendritic cell maturation and contributes to lupus progression. *Adv. Sci.* **2026**, *13*, e08938.

[11] Su, X.; Yu, H.; Lei, Q. Q.; Chen, X. R.; Tong, Y. L.; Zhang, Z. Y.; Yang, W. Y.; Guo, Y. B.; Lin, L. B. Systemic lupus erythematosus: Pathogenesis and targeted therapy. *Mol. Biomed.* **2024**, *5*, 54.

[12] Lazar, S.; Kahlenberg, J. M. Systemic lupus erythematosus: New diagnostic and therapeutic approaches. *Annu. Rev. Med.* **2023**, *74*, 339–352.

[13] Guo, C. P.; Tang, Y. S.; Zeng, L.; You, X. M.; Luo, S. W. E.; Du, Y. F.; Wang, L.; Wang, L. C.; Wang, J. C.; Chen, J. J. et al. Therapeutic potential of lipid nanoparticle-encapsulated CD19-targeting mRNAs in lupus and rheumatoid arthritis. *Adv. Sci.* **2025**, *12*, 2501628.

[14] Xiang, G.; Cui, Y. X.; Wang, P.; Feng, Y. T.; Zhang, C. Y.; Lou, J.; Zhou, X. Nanomedicine targeting the PD-1/PD-L1 axis in autoimmune diseases: Breaking conventional barriers to restore immune tolerance. *J. Nanobiotechnol.* **2025**, *23*, 664.

[15] Ding, C. L.; Shrestha, R.; Zhu, X. J.; Geller, A. E.; Wu, S. Z.; Woeste, M. R.; Li, W. Q.; Wang, H. M.; Yuan, F.; Xu, R. B. et al. Inducing trained immunity in pro-metastatic macrophages to control tumor metastasis. *Nat. Immunol.* **2023**, *24*, 239–254.

[16] Elia, I.; Rowe, J. H.; Johnson, S.; Joshi, S.; Notarangelo, G.; Kurmi, K.; Weiss, S.; Freeman, G. J.; Sharpe, A. H.; Haigis, M. C. Tumor cells dictate anti-tumor immune responses by altering pyruvate utilization and succinate signaling in $CD8^+$ T cells. *Cell Metab.* **2022**, *34*, 1137–1150.e6.

[17] Shan, Q.; Qiu, J. H.; Dong, Z.; Xu, X. T.; Zhang, S. P.; Ma, J.; Liu, S. J. Lung immune cell niches and the discovery of new cell subtypes. *Adv. Sci.* **2024**, *11*, 2405490.

[18] Sattiraju, A.; Kang, S.; Giotti, B.; Chen, Z. H.; Marallano, V. J.; Brusco, C.; Ramakrishnan, A.; Shen, L.; Tsankov, A. M.; Hambardzumyan, D. et al. Hypoxic niches attract and sequester tumor-associated macrophages and cytotoxic T cells and reprogram them for immunosuppression. *Immunity* **2023**, *56*, 1825–1843.e6.

[19] Gu, Y. S.; Bartolomé-Casado, R.; Xu, C.; Bertocchi, A.; Janney, A.; Heuberger, C.; Pearson, C. F.; Teichmann, S. A.; Thornton, E. E.; Powrie, F. Immune microniches shape intestinal $T_{reg}$ function. *Nature* **2024**, *628*, 854–862.

[20] You, S. Y.; Li, S. Q.; Zeng, L. S.; Song, J. S.; Li, Z. F.; Li, W. Y.; Ni, H. X.; Xiao, X.; Deng, W. B.; Li, H. Y. et al. Lymphatic-localized Treg-mregDC crosstalk limits antigen trafficking and restrains anti-tumor immunity. *Cancer Cell* **2024**, *42*, 1415–1433.e12.

[21] Luan, Q. C.; Qiao, R. C.; Wu, X. Y.; Shan, J. Y.; Song, C. H.; Zhao, X. Z.; Zhao, Y. J. Plant-derived Chinese herbal hydrogel microneedle patches for wound healing. *Small* **2024**, *20*, 2404850.

[22] Yang, H.; Song, L.; Sun, B. X.; Chu, D.; Yang, L. L.; Li, M.; Li, H.; Dai, Y.; Yu, Z.; Guo, J. F. Modulation of macrophages by a paeoniflorin-loaded hyaluronic acid-based hydrogel promotes diabetic wound healing. *Mater. Today Bio* **2021**, *12*, 100139.

[23] Guo, P.; Lei, P. K.; Luo, L.; Yang, Q. L.; Yang, Q.; Tian, Y.; Shi, W.; Liu, Y. C.; Zeng, R.; Li, Y. X. et al. Microfluidic-engineered Chinese herbal nanocomposite hydrogel microspheres for diabetic wound tissue regeneration. *J. Nanobiotechnol.* **2024**, *22*, 724.

[24] Liang, F.; Zheng, Y. X.; Zhao, C. C.; Li, L. L.; Hu, Y. Q.; Wang, C. F.; Wang, R. X.; Feng, T.; Liu, X. Y.; Cui, J. R. et al. Microalgae-derived extracellular vesicles synergize with herbal hydrogel for energy homeostasis in osteoarthritis treatment. *ACS Nano* **2025**, *19*, 8040–8057.

[25] Zhang, Q.; Liu, L.; Lin, W. J.; Yin, S. S.; Duan, A. P.; Liu, Z. H.; Cao, W. S. Rhein reverses Klotho repression via promoter demethylation and protects against kidney and bone injuries in mice with chronic kidney disease. *Kidney Int.* **2017**, *91*, 144–156.

[26] Zhang, T. Y.; Liu, P. X.; Shen, W. R.; Li, C.; Zhao, Z. H.; Wu, Y. X.; Sun, T.; Jiang, C. DNase I-mediated chemotactic nanoparticles for NETs targeting and microenvironment remodeling treatment of acute ischemic stroke. *Adv. Sci.* **2025**, *12*, e03689.

[27] He, X. Y.; Gao, Y.; Ng, D.; Michalopoulou, E.; George, S.; Adrover, J. M.; Sun, L. J.; Albrengues, J.; Daßler-Plenker, J.; Han, X. et al. Chronic stress increases metastasis via neutrophil-mediated changes to the microenvironment. *Cancer Cell* **2024**, *42*, 474–486.e12.

[28] Blanco, L. P.; Wang, X. H.; Carlucci, P. M.; Torres-Ruiz, J. J.; Romo-Tena, J.; Sun, H. W.; Hafner, M.; Kaplan, M. J. RNA externalized by neutrophil extracellular traps promotes inflammatory pathways in endothelial cells. *Arthritis Rheumatol.* **2021**, *73*, 2282–2292.

[29] Becatti, M.; Emmi, G.; Bettiol, A.; Mannucci, A.; Argento, F. R.; Fini, E.; Borghi, S.; Nencini, F.; Nicastro, M.; Mattioli, I. et al. Reactive oxygen species -induced modifications of fibrin clots as a link between immune responses and atherothrombosis in systemic lupus erythematosus. *Arthritis Rheumatol.* **2026**, *78*, 344–356.

[30] Chang, L. K.; Xu, Y. L.; Wu, Z. Y.; Shao, Y. C.; Yu, D.; Yang, W. Y.; Ye, L. Y.; Wang, X. Y.; Li, B. B.; Yin, Y. X. Hyaluronic acid methacrylate/laponite hydrogel loaded with BMP4 and maintaining its bioactivity for scar-free wound healing. *Regen. Biomater.* **2023**, *10*, rbad023.

[31] Zhang, J. L.; Chen, C. R.; Fu, H.; Yu, J.; Sun, Y.; Huang, H.; Tang, Y. J.; Shen, N.; Duan, Y. R. MicroRNA-125a-loaded polymeric nanoparticles alleviate systemic lupus erythematosus by restoring effector/regulatory T cells balance. *ACS Nano* **2020**, *14*, 4414–4429.

[32] Zeng, Q.; Wang, S. Y.; Li, M. Y.; Wang, S.; Guo, C. H.; Ruan, X. Y.; Watanabe, R.; Lai, Y. M.; Huang, Y. F.; Yin, X. Y. et al. Spleen fibroblastic reticular cell-derived acetylcholine promotes lipid metabolism to drive autoreactive B cell responses. *Cell Metab.* **2023**, *35*, 837–854.e8.

[33] Voss, K.; Sewell, A. E.; Krystofiak, E. S.; Gibson-Corley, K. N.; Young, A. C.; Basham, J. H.; Sugiura, A.; Arner, E. N.; Beavers, W. N.; Kunkle, D. E. et al. Elevated transferrin receptor impairs T cell metabolism and function in systemic lupus erythematosus. *Sci. Immunol.* **2023**, *8*, eabq0178.

[34] Yoo, E. J.; Oh, K. H.; Piao, H.; Kang, H. J.; Jeong, G. W.; Park, H.; Lee, C. J.; Ryu, H.; Yang, S. H.; Kim, M. G. et al. Macrophage transcription factor TonEBP promotes systemic lupus erythematosus and kidney injury via damage-induced signaling pathways. *Kidney Int.* **2023**, *104*, 163–180.

[35] Lourenço, E. V.; Wong, M.; Hahn, B. H.; Palma-Diaz, M. F.; Skaggs, B. J. Laquinimod delays and suppresses nephritis in lupus-prone mice and affects both myeloid and lymphoid immune cells. *Arthritis Rheumatol.* **2014**, *66*, 674–685.

[36] Li, Y. J.; Liu, H. X.; Yan, H.; Xiong, J. Research advances on targeted-treg therapies on immune-mediated kidney diseases. *Autoimmun. Rev.* **2023**, *22*, 103257.

[37] Parodis, I.; Rovin, B. H.; Tektonidou, M. G.; Anders, H. J.; Malvar, A.; Mok, C. C.; Mohan, C. Lupus nephritis. *Nat. Rev. Dis. Primers* **2025**, *11*, 69.

[38] Li, G. M.; Chen, J. R.; Zhang, H. Q.; Cao, X. Y.; Sun, C.; Peng, F.; Yin, Y. P.; Lin, Z. W.; Yu, L.; Chen, Y. et al. Update on pharmacological activities, security, and pharmacokinetics of rhein. *Evid. Based Complement. Alternat. Med.* **2021**, *2021*, 4582412.

[39] Hosseinnejad, A.; Ludwig, N.; Wienkamp, A. K.; Rimal, R.; Bleilevens, C.; Rossaint, R.; Rossaint, J.; Singh, S. DNase I functional microgels for neutrophil extracellular trap disruption. *Biomater. Sci.* **2022**, *10*, 85–99.

[40] Yuan, X.; Long, L. S.; Wang, M. H.; Chen, W. H.; Liang, B. E.; Xu, L.; Wang, W. D.; Li, C. L. Rhein alleviates cisplatin-induced acute kidney injury via downregulation of NOX4-COX2/PGFS signaling pathway. *Drug Des. Devel. Ther.* **2025**, *19*, 4641–4664.

[41] Zhang, Z. H.; Peng, S. J.; Xu, T. Y.; Liu, J.; Zhao, L. E.; Xu, H.; Zhang, W.; Zhu, Y. Y.; Yang, Z. M. Retinal microenvironment-protected rhein-GFFYE nanofibers attenuate retinal ischemia-reperfusion injury via inhibiting oxidative stress and regulating microglial/macrophage M1/M2 polarization. *Adv. Sci.* **2023**, *10*, 2302909.

This is an open access article under the terms of the Creative Commons Attribution 4.0 International License (CC BY 4.0, https://creativecommons.org/licenses/by/4.0/).

© The Author(s) 2026. Published by Tsinghua University Press.